



Evidence of Absence of Tidal Features in the Outskirts of Ultra Diffuse Galaxies in the Coma Cluster

Lamiya Mowla¹ , Pieter van Dokkum¹ , Allison Merritt¹ , Roberto Abraham² , Masafumi Yagi³ , and Jin Koda⁴

¹Astronomy Department, Yale University, New Haven, CT 06511, USA; lamiya.mowla@yale.edu

²Department of Astronomy and Astrophysics, University of Toronto, 50 St. George Street, Toronto, ON M5S 3H4, Canada

³Optical and Infrared Astronomy Division, National Astronomical Observatory of Japan, Mitaka, Tokyo, 181-8588, Japan

⁴Department of Physics and Astronomy, Stony Brook University, Stony Brook, NY 11794-3800, USA

Received 2017 July 7; revised 2017 September 26; accepted 2017 October 7; published 2017 December 7

Abstract

We study the presence of tidal features associated with ultra diffuse galaxies (UDGs) in galaxy clusters. Specifically, we stack deep Subaru images of UDGs in the Coma cluster to determine whether they show position angle twists at large radii. Selecting galaxies with central surface brightness $\mu(g, 0) > 24 \text{ magarcsec}^{-2}$ and projected half-light radius $r_e > 1.5 \text{ kpc}$, we identify 287 UDGs in the Yagi et al. catalog of low surface brightness Coma objects. The UDGs have apparent spheroidal shapes with median Sérsic index $\langle n \rangle = 0.8$ and median axis ratio $\langle b/a \rangle = 0.7$. The images are processed by masking all background objects and rotating to align the major axis before stacking them in bins of properties such as axis ratio, angle of major axis with respect to the cluster center, and separation from cluster center. Our image stacks reach further than 7 kpc ($\gtrsim 4r_e$). Analysis of the isophotes of the stacks reveals that the ellipticity remains constant up to the last measured point, which means that the individual galaxies have a non-varying position angle and axis ratio and show no evidence for tidal disruption out to $\sim 4r_e$. We demonstrate this explicitly by comparing our stacks with stacks of model UDGs with and without tidal features in their outskirts. We infer that the average tidal radius of the Coma UDGs is $> 7 \text{ kpc}$ and estimate that the average dark matter fraction within the tidal radius of the UDGs inhabiting the innermost 0.5 Mpc of Coma is $> 99\%$.

Key words: galaxies: clusters: individual (Coma) – galaxies: photometry – galaxies: structure

1. Introduction

Ultra diffuse galaxies (UDGs) are extended low surface brightness galaxies with half-light radii comparable to those of L_* galaxies and stellar masses comparable to those of dwarf galaxies. UDGs were defined empirically as galaxies with central surface brightness $\mu(0, g) > 24 \text{ magarcsec}^{-2}$ and projected half-light radius (the radius containing 50% of the light) $r_e > 1.5 \text{ kpc}$ (van Dokkum et al. 2015a). Given their low stellar masses, it has been argued that UDGs may be analogs of other low-mass galaxies, which have been puffed up by gravitational heating, tidal effects, or a high angular momentum (e.g., Amorisco & Loeb 2016; Beasley & Trujillo 2016). An alternative idea is that many are failed galaxies that quenched earlier than other galaxies of the same halo mass, through ram pressure stripping, stellar feedback driven galactic winds, or other effects (van Dokkum et al. 2015b; Yozin & Bekki 2015; Agertz & Kravtsov 2016; Beasley et al. 2016; Di Cintio et al. 2017; Peng & Lim 2016). Some UDGs have very high M/L ratios as determined from their kinematics (Beasley & Trujillo 2016; Trujillo van Dokkum et al. 2016). However, whether the majority of UDGs form a stable population or whether many are part of a disrupting population of galaxies mixing in with the intracluster and intragroup light (Searle & Zinn 1978) is still an outstanding question.

As galaxies move through the cluster, they are disturbed due to the tidal field of the cluster and interactions with other galaxies. The effect is strongest beyond the tidal radius, where the gravitational force from the enclosed mass of the galaxy equals the gravitational force produced by the cluster. The tidal

radius r_t is given by

$$r_t = R \left(\frac{m}{3M} \right)^{1/3}, \quad (1)$$

where R is the distance from the cluster center, M is the total mass enclosed by the cluster within radius R , and m is the total mass of the galaxy within radius r_t (King 1962). Beyond the tidal radius, stars can escape, giving rise to low surface brightness tidal tails in a characteristic “S”-shaped pattern (see Johnston et al. 2002, 2008; Bullock & Johnston 2005; Koch et al. 2012, and Figure 1). Hence, the tidal radius can be determined by identifying the radius at which tidal tails appear, which in turn can be used to calculate the enclosed mass of the object (Penny et al. 2009).

Imaging even the central regions of individual UDGs is challenging. This is demonstrated in Figure 3 of van Dokkum et al. (2017), which shows deep *HST* images of UDGs in Coma: only the light within $\lesssim r_e$ is readily visible. An alternative to ultra-deep imaging is stacking a large number of galaxies with similar properties to greatly improve the overall depth reached at the cost of losing information of individual galaxies (Zibetti et al. 2004; van Dokkum et al. 2010; Tal & van Dokkum 2011; D’Souza et al. 2014). The stacking technique requires deep images of a large number of galaxies with similar properties (Zibetti et al. 2004). In this paper, we are stacking deep *R*-band images of 231 UDGs in the Coma cluster from Suprime-Cam on the Subaru Telescope (Koda et al. 2015; Yagi et al. 2016). We use the fact that tidal tails produce a change in the position angle of isophotes to constrain their prominence. We simulate model galaxies with

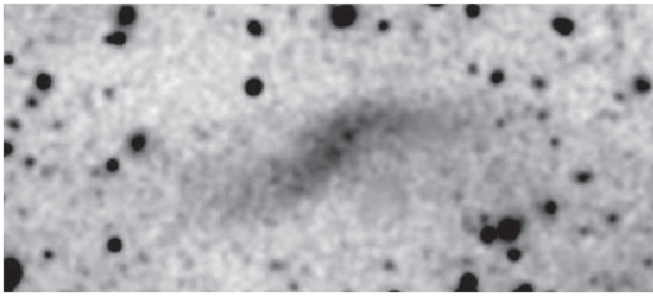


Figure 1. Example of a tidally disrupted galaxy (not a UDG) with an “S”-shaped morphology. This is a co-added V and I image of the galaxy HCC-087 in the Hydra I cluster, taken from Koch et al. (2012). The image covers $1.^{\circ}6 \times 0.^{\circ}7$ ($\sim 22 \times 10$ kpc).

and without tidal tails to test their effect on stacked images and compare them to UDG stacks. The radius at which tidal tail signatures appear allows us to estimate the observed average tidal radius of Coma UDGs and if no signatures are found, we obtain a lower limit to the tidal radius. Using the tidal radius, we can determine the average minimum enclosed mass of the stacked galaxies depending on their position in the cluster.

2. Data and Sample Selection

2.1. Data

The cluster UDG sample for this study is a sub-sample of the 854 low surface brightness galaxies (LSB galaxies) found in the Coma cluster by Koda et al. (2015) using deep *R*-band images, obtained with Suprime-cam on the Subaru telescope (Okabe et al. 2014). The selection criteria in that study were set such that all 47 of the Dragonfly UDGs were recovered, which included objects that are smaller than the canonical UDG criterion of $r_e > 1.5$ kpc.⁵ Details of the reduction procedure and how the objects were selected are given in Yagi et al. (2016).

2.2. GALFIT fitting

We ran GALFIT (Peng et al. 2002, 2010) on 201 pixel \times 201 pixel ($40.^{\circ}6 \times 40.^{\circ}6$) image cut-outs centered on the LSB galaxies to derive the physical parameters of the objects. All foreground and background objects, including point sources inside the LSB galaxies, were masked in the fits. Masks were created using the segmentation map from SExtractor (Bertin & Arnouts 1996) in two stages. In stage one, we ran SExtractor on the individual stamps with a fixed detection threshold of 1.5 times the standard deviation above the background rms level, 32 deblending sub-thresholds, and a minimum contrast parameter of 0.005. We also created FLAG maps for the images by flagging pixels at the edges of frames. All objects in the segmentation map except the center of the LSB galaxy were masked in the primary mask. Using the primary mask as the bad pixel map, we used GALFIT to fit a one-component Sérsic profile to the LSB galaxy as an initial model. In stage two, the residual map of the initial fit was used to create a second segmentation map with SExtractor with the deblending threshold raised to 64 and contrast parameter lowered to 0.001. This stage preferentially detects smaller and fainter objects that overlap with the (now-removed) LSB galaxy. The

final mask is made by adding these two masks so that any bright objects other than the smooth component of the LSB galaxy are masked in the final image. Using this final mask as the bad pixel map, GALFIT is used to fit a single-component Sérsic profile with Sérsic index and sky background allowed to vary. We judged the fits acceptable based on the goodness-of-fit (χ^2/ν) < 1.2 and by visual inspection of the model fits. Using the physical parameters from the GALFIT fit of each LSB galaxy, we select our UDG sample with the following definition of UDGs: $r_e > 1.5$ kpc and $\mu(0, R) > 23.5$ magarcsec $^{-2}$ (van Dokkum et al. 2015b). The surface brightness cut was determined assuming a typical UDG color of $g - R \approx 0.5$ (see van Dokkum et al. 2015b). From the 857 LSB galaxy galaxies, 287 objects satisfy the UDG criterion and were selected to form our sample of Coma UDGs.

2.3. Properties of Coma UDGs

Figure 2 shows the distribution of the physical parameters from our GALFIT fits of the UDGs in the Coma cluster. The median central surface brightness $\mu(0, R)$ of the UDGs is 24.6 ± 0.1 magarcsec $^{-2}$, where the error is computed by bootstrap re-sampling. The median Sérsic index is 0.88 ± 0.02 with 80% UDGs having n between 0.6 and 1.1, in agreement with other studies (Koda et al. 2015; van der Burg et al. 2016; Román & Trujillo 2017). The median axis ratio is 0.71 ± 0.01 , identical to the value found by Koda et al. (2015), with a quarter of the UDGs having $b/a < 0.6$. The median projected distance, R_c , of the UDGs from the cluster center is 1 ± 0.1 Mpc. There are fewer UDGs within 250 kpc of the cluster center; this may be an observational bias due to the brightness of the ICL or a true deficit and is consistent with other UDG studies (Beasley & Trujillo 2016; van der Burg et al. 2016). The UDGs near the center of the cluster are slightly rounder than those in the outskirts, with median $b/a = 0.75$ for UDGs with $R_c < 0.65$ Mpc and $b/a = 0.68$ for UDGs with $R_c > 1.5$ Mpc. The projected orientation of the major axis of UDGs relative to the cluster-centric direction is also shown in Figure 2, where θ_c is the angle between the major axis of the UDG and the line connecting the galaxy to the center of the cluster. Here, $\theta_c = 0^\circ$ means the major axis aligns in the cluster-centric direction while $\theta_c = 90^\circ$ means the minor axis aligns in cluster-centric direction. Again, a slightly bigger axis ratio is found for UDGs that are pointed toward the cluster center than those that are tangential to it, with median $b/a = 0.78$ for UDGs with $\theta_c < 25^\circ$ and $b/a = 0.69$ for UDGs with $\theta_c > 50^\circ$.

3. Analysis

3.1. Stacking

The UDGs were divided in bins based on various properties, and the images of UDGs in each bin were processed and added together to create stacked images. For the stacking analysis, we used UDGs with $r_e < 2.5$ kpc to ensure we are adding light from similar-sized objects. The 231 UDGs that satisfy this criterion were visually inspected and used in the stacking analysis. The pre-stacking processing includes:

1. Shift the image to center the UDG on the central pixel;
2. Rotate the image to align the major axis of the UDG with the y-axis;

⁵ In this paper, we distinguish the generic term “low surface brightness galaxies” and the term “ultra diffuse galaxies” (UDGs). UDGs have $\mu(0, g) > 24$ and $r_e > 1.5$ kpc. The Yagi et al. catalog contains many low surface brightness galaxies that are not UDGs according to this definition.

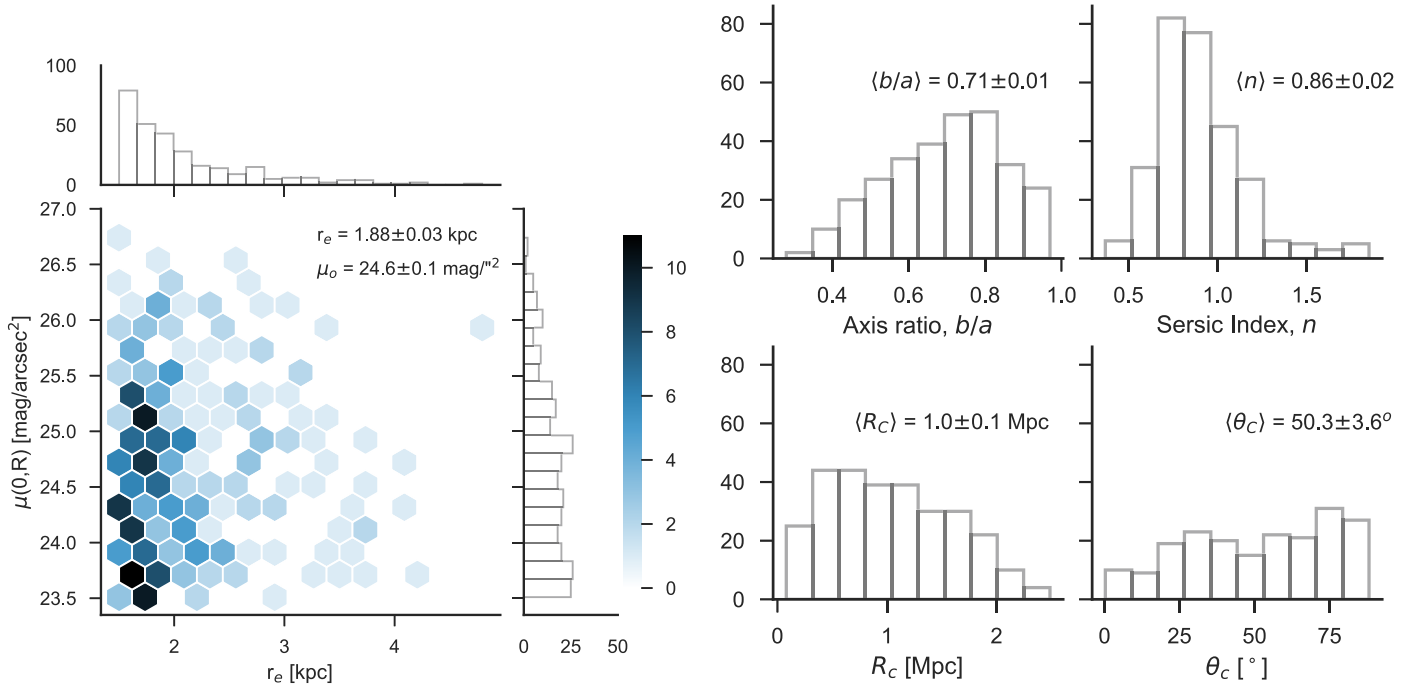


Figure 2. Histograms of effective radii r_e , central surface brightness $\mu(R, 0)$, axis ratio b/a , Sérsic index n , angle between the major axis and the cluster-centric direction θ_C , and distance from the cluster center R_C ($\alpha = 12^{\text{h}}59^{\text{m}}35\overset{\text{s}}{.}7$ and $\delta = 27^{\circ}57'34''$). The left plot shows the distribution of r_e and $\mu(0, R)$ of the UDGs illustrating the selection criteria of $r_e > 1.5$ kpc and $\mu(0, R) > 23.5$ mag/arcsec $^{-2}$. The median values for each of the parameters and the bootstrap errors of the median values are shown on the plots. In the last histogram for the cluster-centric angle, UDGs whose $b/a < 0.8$ are used only. Here, $\theta_C = 0^\circ$ means the major axis of UDG is aligned with the cluster-centric direction, and $\theta_C = 90^\circ$ means the minor axis is aligned with the cluster-centric direction.

3. Apply the final mask created in the GALFIT stage (Section 2.2) to mask any foreground/background objects, including point sources on the UDG;
4. Subtract the average sky count found by GALFIT from the image.

The processed image has only the smooth component of the UDG light centered and vertically aligned along the major axis. The UDGs were binned in ranges of b/a , θ_C , and R_C to investigate any correlations of these properties with the presence of tidal features. We did not re-scale the sizes of the galaxies prior to stacking them but the images were normalized by the total flux from the GALFIT model. This normalization ensures that the stacks are not dominated by the brighter and larger UDGs. Stacks were created by adding together the processed images in each bin. The object masks were also summed to create weight maps, and the summed image was divided by its respective weight map to create averaged exposure-corrected stacks. The background subtraction is somewhat uncertain as the images show a very faint negative “bowl” around all objects; this is a common artifact of over-subtraction of background during reduction of images of extended objects. We address this by applying a final background correction after stacking, by determining the median count at $R = 8.5$ kpc, and subtracting this value. Effectively, we set the galaxy flux to zero at this radius. This uncertainty in the background value is important for studies of the outer surface brightness profile, but is expected to have a negligible effect on the ellipticity profile.

3.2. Mock Galaxy Images

We made mock images for the 231 UDGs to test the effect of tidal features in stacked images. Two types of model UDGs were

created: (i) Sérsic, and (ii) Warped. The Sérsic model is a simple ellipse with Sérsic light profile and isophotes with constant axis ratio and position angle. This is the same as the GALFIT model of the galaxy. Simulations of tidally distorted galaxies typically show breaks in the surface brightness profile where the tidal tails begin (see Johnston et al. 2002). Our Warped model reproduces this feature along with the the axis ratios and position angles of the isophotes changing with radius. They are made by summing 100 ellipses with Sérsic light profiles, with their axis ratio, Sérsic index, central surface brightness, and position angle changing with radius to create S-shaped isophotes beyond ∼2 r_e . One hundred models are made for each UDG with a random combination of values for the starting r_e , b/a , n , μ_0 within 0.5 times the true values of the respective parameters for the UDG. GALFIT is run on the 100 models, and the model with fitted parameters that are closest to those of the observed UDG is chosen as the best Warped model. If a GALFIT parameter of the best-fit model is more than 20% different from that of the observed UDG, then the model is rejected and the process is repeated by making 100 more models. The masks for each UDG are used as bad pixel maps during the GALFIT fit of Warped model so as to take into account the effect of masking on the fit. The end result is that we have a Warped model for each UDG that produces the same GALFIT parameters as were actually measured for that UDG, as illustrated in Figure 3. The direction of the warp is chosen at random, with the constraint that there are approximately equal numbers of UDG models with a warp in each direction. Details for creating images of Warped models are given in Appendix.

The bottom panel of Figure 3 shows the Warped model with their respective sky background and mask added. As can be seen, GALFIT and our eyes cannot distinguish between the top and the bottom panel even though the underlying light profiles

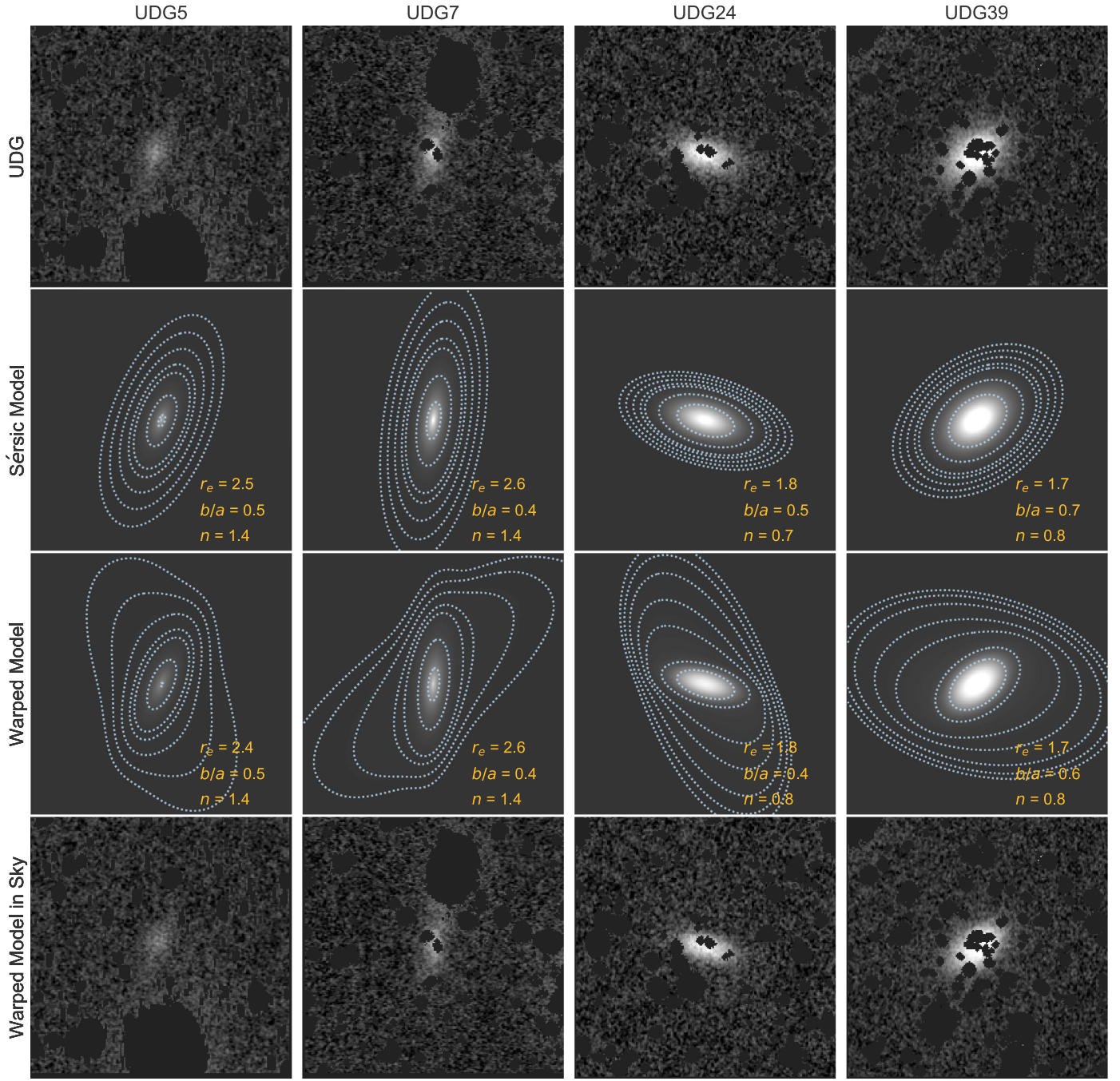


Figure 3. Images of UDGs and their respective models with and without tidal tails. The top panels show Subaru R -band images of UDGs in the Coma cluster, with foreground and background objects including point sources inside the UDG masked. The names of the UDGs correspond to their IDs in the Yagi et al. (2016) catalog. The stamps span $40\text{''}6 \times 40\text{''}6$ (19 kpc \times 19 kpc at the distance of Coma; scale length $0.47 \text{ kpc arcsec}^{-1}$). The second panel shows the Sérsic models of UDGs as determined by GALFIT. The third panel shows the Warped model of galaxies with S-shaped light profile. The effective radius r_e , axis ratio b/a , and Sérsic index n from the GALFIT fits for each of the images are shown. The dotted contours show the isophotes. The bottom panel shows the Warped model of each UDG with their corresponding sky background and mask added for visual comparison with the UDG image in the top panel.

of the galaxies are significantly different. Due to the very low S/N of the UDGs methods such as fitting ellipses to trace the isophotes fail for individual UDGs. Conventional methods cannot trace the presence of tidal features of UDGs necessitating the use of stacking.

3.3. Ellipse Fitting

The radial variation of the average structure of the galaxies is determined by fitting elliptical isophotes to the stacked images.

The fits are performed using the IRAF task *ellipse*, with logarithmic spacing of ellipses. The center position, axis ratio, and position angle are allowed to vary with radius in the fits.

4. Results

4.1. Stack of Elongated UDGs

The key result of our study is shown in the top panel of Figure 4, which shows the observed axis ratio as a function of radius for the stack of the 68 UDGs with $b/a < 0.6$ (pink

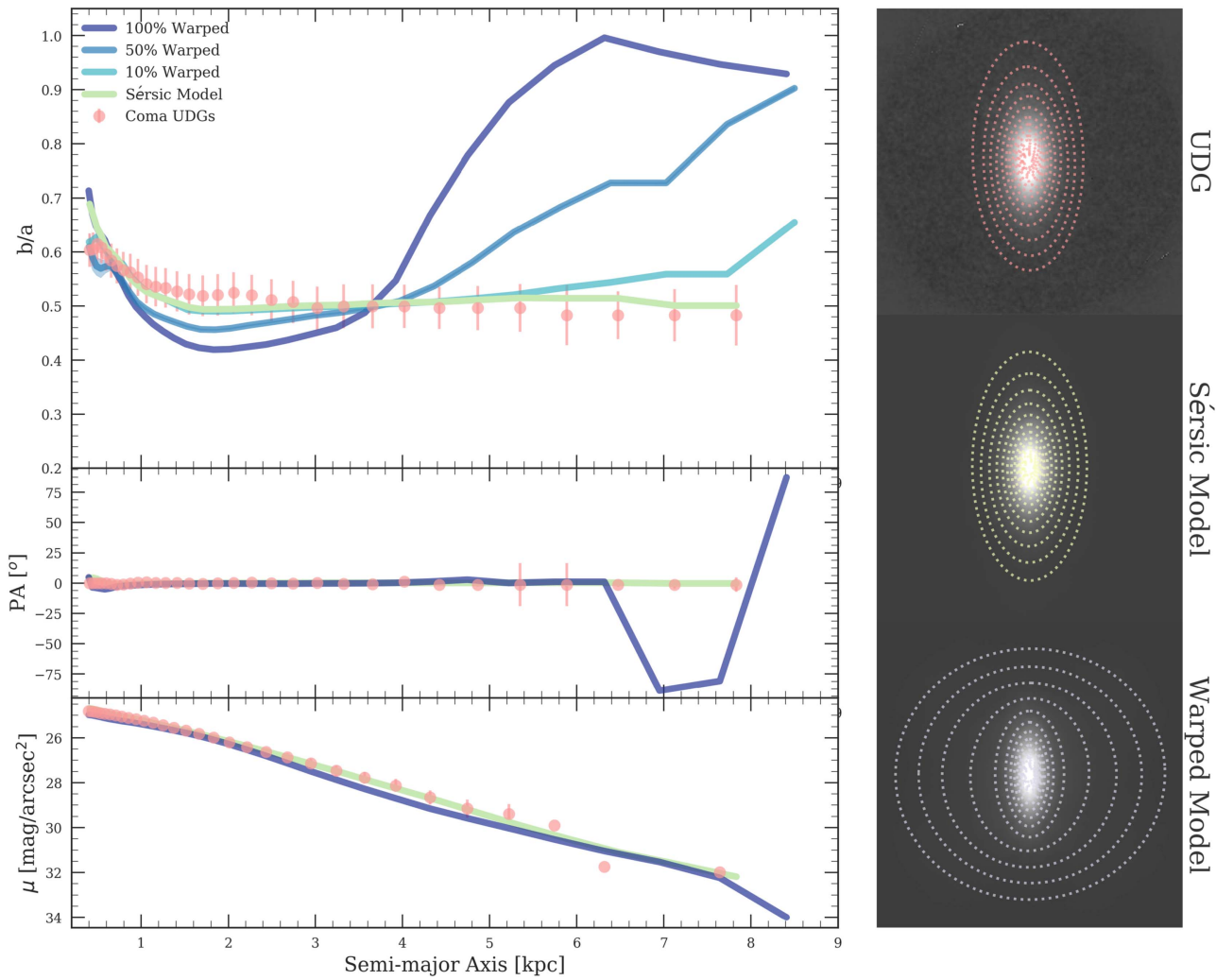


Figure 4. The axis ratio b/a , position angle PA, and surface brightness μ of the successive elliptical isophotes fitted on the stacked images with the IRAF task ELLIPSE are shown in the left panels. The stacked images are shown in the right panels, overplotted with their elliptical isophotes.

points with error bars). We focus on this sub-sample, as the most elongated UDGs are the most sensitive to tidal features (as the fractional change in b/a with radius is higher for UDG with smaller axis ratio). The axis ratio is nearly constant with radius out to the last measured point at $r \sim 8$ kpc. This is remarkable, as it implies that the individual galaxies going into the stack are coherent, with the same axis ratio and position angle, out to this radius.

This is quantified and illustrated by comparing the observed stack to the two model stacks: the Sérsic model, which is built from individual galaxies that have a constant ellipticity and position angle, and the Warped model, which is built from individual galaxies with “S”-shaped tidal distortions. The right panel shows the Sérsic and Warped stacks overlaid with their isophotes from the ellipse-fitting analysis, while the left panel shows the axis ratio, position angle, and surface brightness of the elliptical isophotes. As expected, the axis ratio of the stack of Sérsic models remains nearly constant at 0.50 ± 0.05 . However, the axis ratio of the stack of Warped models (shown by the 100% Warped model line) increases from 0.50 ± 0.05 to 1.0 ± 0.05 between $4 \text{ kpc} < a < 8 \text{ kpc}$. This behavior is expected: when the S-shaped images of the Warped models are added together in a stack, the resulting light profile has a

circularized profile in the outskirts. Axis ratios of stacks with different fractions of Sérsic and Warped models are also plotted to show the effect on the average axis ratio of the isophotes if only a small fraction of UDGs are disrupting. We compute the error bars in the axis ratio, position angle, and surface brightness by bootstrap re-sampling of the stacks. The error bars for the models are shown as shaded regions, which are barely visible due to their small sizes ($\sim 2\%$). For the 10% and 50% Warped stacks, we created 500 instances of stacks with different combinations of Warped and Sérsic models and found $< 3\%$ change in the results of the ELLIPSE analysis. This shows that the results are not dependent on the disruption of any particular galaxy. The stacked axis ratio of the observed UDGs closely follows the non-warped Sérsic model out to the last measured point at ~ 8 kpc. In order to test whether larger UDGs were dominating the light in the outskirts from smaller UDGs, we also stacked the UDGs in bins of r_e and found no significant change in axis ratio at larger radii in any of the size bins. Hence, our conclusion remains unchanged even when we add UDGs with $r_e > 2.5$ kpc.

Note that all models reproduce the small scale variations in the ellipticity profile within ~ 1.5 kpc. This is because the PSF and the same masks have been applied to the models as to the

Table 1
Number of UDGs in Each Stack

Property	Bin	Number of UDGs	$\langle b/a \rangle^a$
Axis ratio	$b/a \leq 0.6$	68	0.50 ± 0.07
	$0.6 < b/a < 0.8$	85	0.71 ± 0.06
	$b/a \geq 0.8$	78	0.86 ± 0.07
Cluster-centric angle ^b	$\theta_c \leq 45^\circ$	62	0.59 ± 0.15
	$\theta_c > 45^\circ$	70	0.59 ± 0.14
Distance from cluster center ^b	$R_c \leq 1.0 \text{ Mpc}$	67	0.63 ± 0.12
	$R_c > 1.0 \text{ Mpc}$	67	0.59 ± 0.13

Notes.

^a Median axis ratio of the stack.

^b Only UDGs with $b/a < 0.75$ used in the stack.

observations. We tested this by creating stacks of models without any masks or PSF, with the resulting isophotes having perfectly smooth shapes. The middle panel of Figure 4 shows the position angles of the isophotes of the stacks. Because all of the UDGs and models are rotated such that their major axes are aligned with the y-axis, the average position angle of the stack remains at zero for all of the stacks. The change in the position angle of the Warped stacks beyond 7 kpc indicates that, at this radius, the strength of the warps causes the stack to be slightly more extended along the (original) minor axis than along the major axis, as can be seen in the image of the Warped model. The bottom panel shows the surface brightness of the isophotes. This has an almost exponential profile going from $24 \text{ magarcsec}^{-2}$ to $>30 \text{ magarcsec}^{-2}$, although we caution that our straightforward background subtraction makes the interpretation difficult.

4.2. Stacking Sub-samples of UDGs

In Section 4.1 we stacked the UDGs with the smallest axis ratios, finding no evidence for tidal distortions. Here, we analyze other sub-samples of UDGs, to determine whether there is an increase in the stacked axis ratio with radius for any of them. Table 1 shows the number of UDGs in each sub-sample stack and the median axis ratio of each stack. We first consider other axis ratio bins, that is, the average radial trend of the axis ratio at large radii for galaxies with different GALFIT-determined axis ratios in their inner parts. The top panel of Figure 5 shows the radial behavior of the axis ratio for four stacks with different GALFIT-determined axis ratio. The dots with error bars show the UDG stack, the darker line shows the Sérsic model stack, and the light line shows the Warped model stack. Each stack contains 60–85 UDGs. As expected, for the Sérsic models, the axis ratio of the isophotes remain constant at the median axis ratio of the stack while the Warped model axis ratio rises at >4 kpc in all three stacks, with the effect being the strongest for the thinnest UDGs. The observed axis ratio closely follows the Sérsic model stack except for the $0.6 < b/a < 0.8$ bin, which has some irregularity beyond radius >4.5 kpc but follows the Sérsic model within two standard deviations. The median residual is for the Sérsic model (-0.01) is smaller than the median residual for the Warped model (-0.10).

Next, we test whether UDGs whose major axes are (mis-)aligned with the cluster-centric direction are preferentially

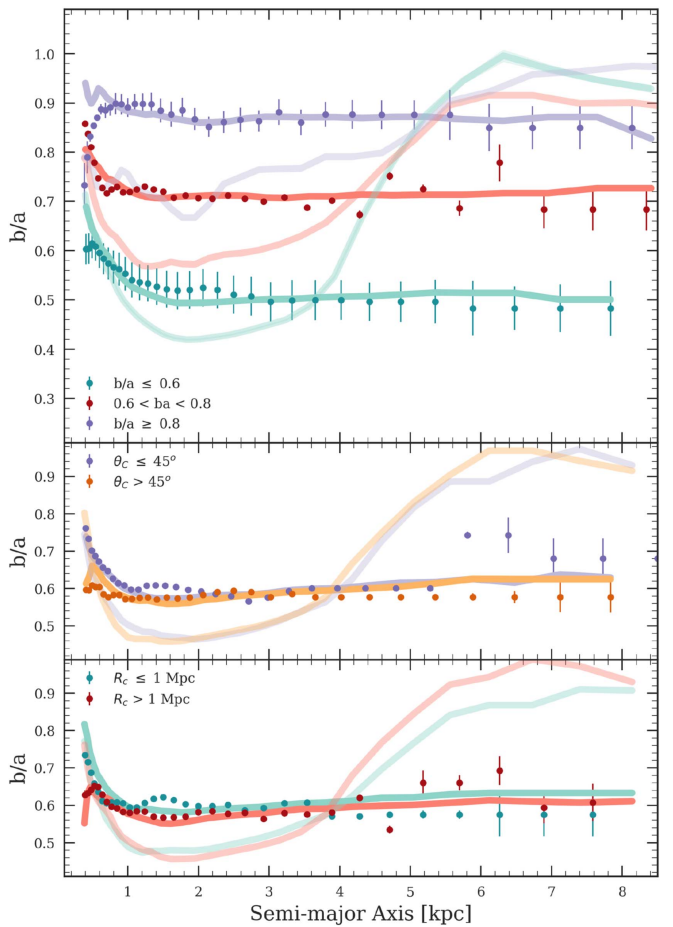


Figure 5. The axis ratios of the isophotes of the different stacks made in bins of different properties: axis ratio (top panel), angle of the major axis with respect to the direction toward the cluster center (middle panel), and distance from the cluster center (bottom panel). The dots show the UDG data, the darker line shows the Sérsic model, and the lighter line shows the Warped model. With the possible exception of galaxies with $\theta_c < 45^\circ$, the axis ratio remains constant with radius in all sub-samples.

tidally disrupted. This is parameterized by the projected angle, θ_c , between the major axis of the UDG and the line connecting the UDG with the center of the cluster. For UDGs whose major axis points toward the center of the cluster $\theta_c = 0$ (for $\theta_c = 90^\circ$ the major axis is perpendicular to the direction toward the cluster center, and the minor axis points to the cluster center). For each of the stacks, only galaxies with $b/a < 0.7$ are included so that the position angle of the major axis is well-determined. The UDGs with major axis aligned with the cluster center ($\theta_c < 45^\circ$) are in purple and those with minor axis aligned with the cluster center ($\theta_c > 45^\circ$) are in orange. Both stacks have similar median axis ratio with the UDGs pointed toward the cluster center with $b/a = 0.6 \pm 0.03$ and the UDGs tangential with the cluster center with $b/a = 0.59 \pm 0.03$. The slight irregularity beyond >4.5 kpc for the $\theta_c > 45^\circ$ stack as well as for the $0.6 < b/a < 0.8$ stack from the above panel can be attributed to distortions in the galaxies that are not modeled by our S-shaped Warped model.

Finally, we determine whether UDGs that are closer to the center of the cluster are more disrupted than those at larger distances. This might be expected, as tidal forces are stronger near the center than in the outskirts. The bottom panel of

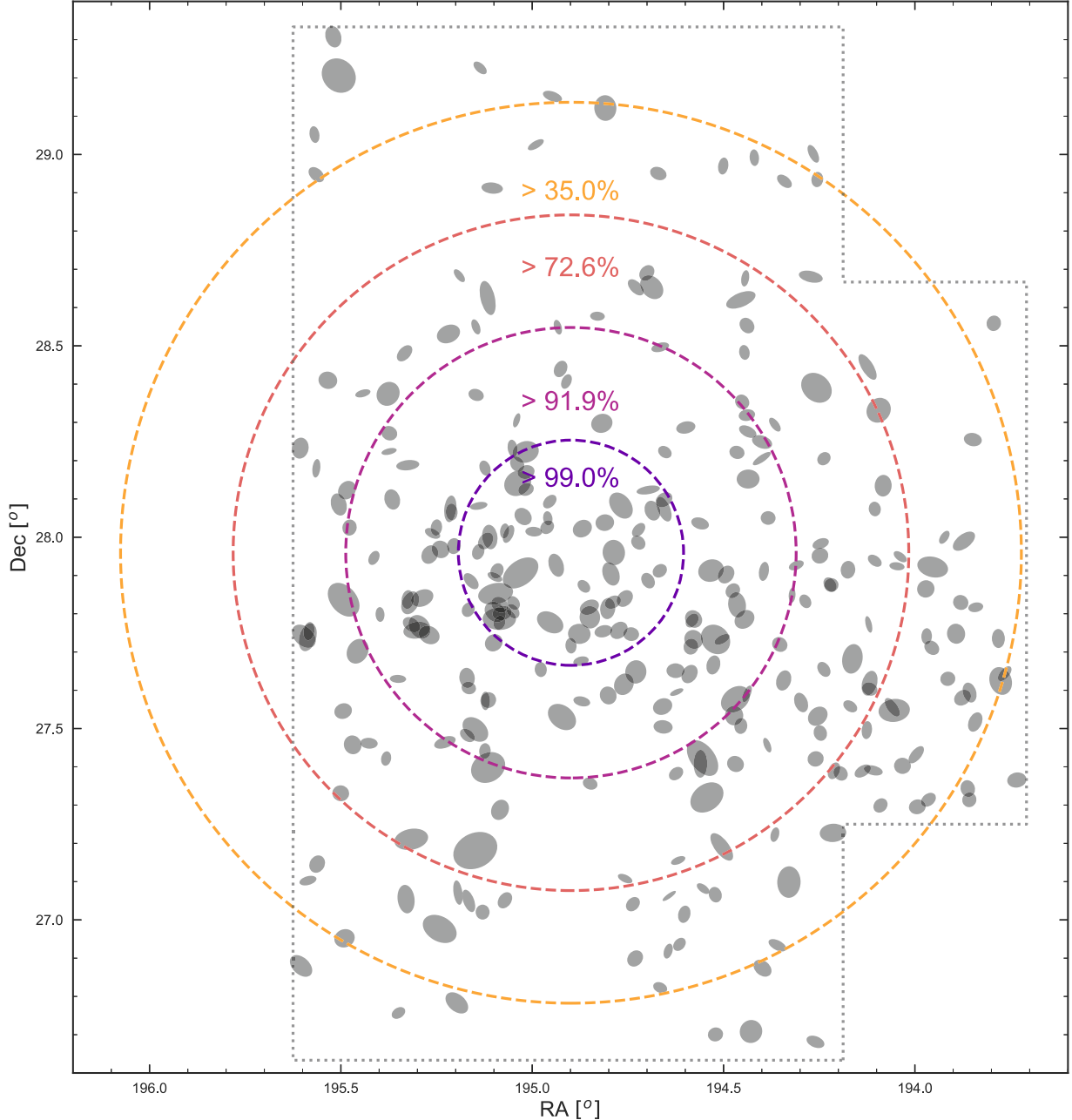


Figure 6. Spatial distribution of UDGs in the Coma cluster. The axis ratio and relative sizes of the ellipses represent the GALFIT fit values of our UDG sample (with the symbol size magnified by a factor of 20). The dotted gray line traces the field covered by the Subaru imaging with a total area of 4.1 deg^2 (Okabe et al. 2014). The dashed circles represent the 0.5, 1.0, 1.5, and 2.0 Mpc separation from the cluster center at the distance of Coma cluster. Using our estimated tidal radius of 7 kpc, the total mass enclosed within the tidal radius is calculated using Equation (2) for each of the separation bins marked by the dashed lines. From the calculated enclosed mass and assuming stellar mass $M_{\text{star}} \approx 1.1 \times 10^8 M_{\odot}$, the minimum dark matter required in order for the UDG to not be tidally disrupted is estimated. The minimum dark matter fractions for the UDGs within each separation bin are shown on the plot.

Figure 5 shows the stacks of the UDGs with the smaller projected distance to the cluster center ($R_c < 1.0 \text{ Mpc}$ in green) and those with largest projected distance from the cluster center ($R_c > 1.0 \text{ Mpc}$ in red). Again, a slight irregularity beyond $>4.5 \text{ kpc}$ is noticed for the $R_c > 1 \text{ Mpc}$ stack, showing presence of some distortion; but overall, both the stacks follow the Sérsic model stack. We note that θ_c and R_c are projected properties; trends with the physical distance of a galaxy to the center of the cluster, or the three-dimensional vector connecting a galaxy to the cluster center, will necessarily be somewhat diluted in projection.

5. Discussion and Conclusions

We have demonstrated that the stacking technique can recover simulated tidal features: models with an artificially induced S-shaped tidal distortion beyond $\sim 2r_e$ (4 kpc) show a pronounced increase in the observed axis ratio of the stack (see Figure 4). We selected UDGs with $r_e < 2.5 \text{ kpc}$ for our stacking analysis. The increase in axis ratio in stacked images is not seen in the data: the axis ratio profile remains flat out to the last measured point at $\sim 7.5 \text{ kpc}$, or $>4\langle r_e \rangle$. We conclude that the tidal radius of the majority of Coma UDGs likely lies

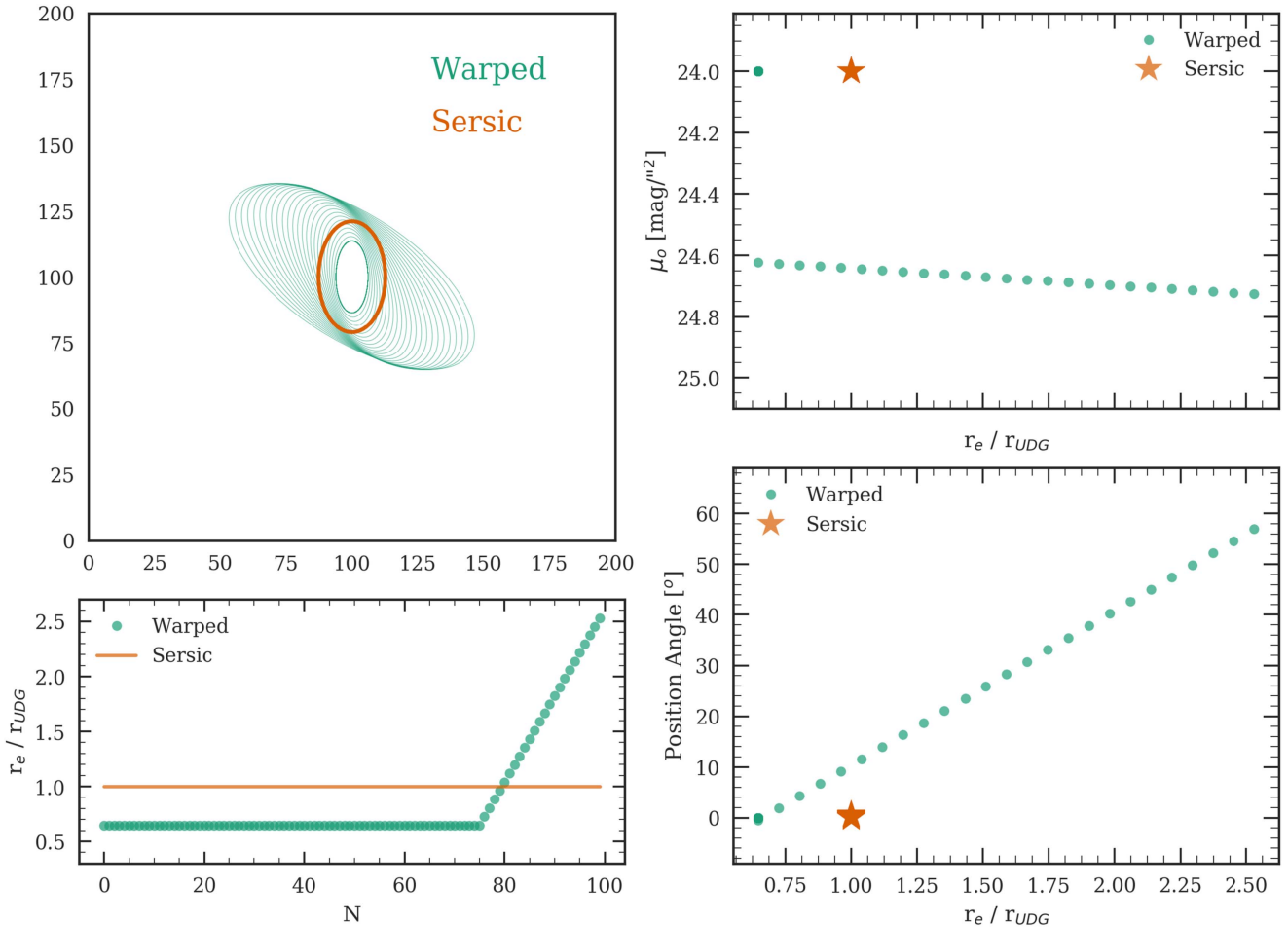


Figure 7. Making Sérsic and Warped models with overlapping ellipses. The left panel shows the position of the ellipses making up the Sérsic and the Warped model (top) and the change in the effective radius of the consecutive ellipses (r_e) normalized by the effective radius of the UDG modeled (r_{UDG} ; bottom). The models are rotated by PA_{UDG} to align the major axis with the y-axis. Each model is made up of 100 ellipses, with Sérsic light profiles having the same center. The effective radii of the ellipses in the Sérsic model remain constant at the effective radius of the UDG (r_{UDG}) being modeled. The Warped models are created by adding an inner component with a fixed position angle to an outer component with position angles varying with radius. The inner component has a fixed effective radius (r_{in}) smaller than r_{UDG} , while the outer component has effective radius (r_{out}) that increases with N from r_{in} to $\sim 5r_{in}$. The right panel shows central surface brightness (top) and position angle (bottom) of the ellipses as a function of normalized effective radius of the ellipses r_e / r_{UDG} . In the Sérsic model, all of the ellipses have the same central surface brightness and position angle, equal to the value of the UDG being modeled. For the Warped model, the inner components have the same central surface brightness and position angle as the UDG. For the outer component, the ellipses get fainter and their position angle increases by up to 60° .

beyond this point and determine a lower limit of $r_t \gtrsim 7$ kpc for most UDGs.

With our estimated tidal radius of the majority of galaxies, we can now calculate the average enclosed mass within the tidal radius, depending on their position in the cluster. Rewriting Equation (1),

$$m = 3M \left(\frac{r_t}{R} \right)^3 \quad (2)$$

the enclosed mass of the UDGs within the tidal radii can be estimated, where $M = 1.88 \times 10^{15} h^{-1} M_\odot$ and $R = 1.99 h^{-1}$ Mpc, the virial mass and the virial radius of the Coma cluster, respectively (Kubo et al. 2007). This means for a UDG at a distance of 0.5 Mpc from the cluster center, the mass enclosed within the tidal radius is $\gtrsim 1.6 \times 10^{10} M_\odot$. The median absolute R -band magnitude $\langle M_R \rangle = 14.1$, and we estimate the median stellar mass of all UDGs $\langle M_{star} \rangle \sim 1.1 \times 10^8 M_\odot$, calculated by scaling to the stellar mass estimate of the Coma cluster UDGs in van Dokkum et al. (2015b). The dark matter fraction of these innermost UDGs within is then $\gtrsim 99\%$ within 7 kpc. Because our

stacks of galaxies in bins of distance from the cluster center did not show any sign of tidal tail for the UDGs closest to the cluster center, we are assuming that these central UDGs also have tidal radius $\gtrsim 7$ kpc. Figure 6 shows the minimum dark matter fraction of UDGs in the Coma cluster depending on their position in the cluster.⁶ The high dark matter fractions that we derive are consistent with estimates based on dynamics (Beasley et al. 2016; van Dokkum et al. 2016) and globular cluster counts (Beasley et al. 2016; Peng & Lim 2016; van Dokkum et al. 2016).

Irrespective of the quantitative constraints on the dark matter fraction, the qualitative conclusion from this study is that we can rule out that most cluster UDGs resemble objects such as HCC-087 (Figure 1). This result does not rule out that a small fraction of the cluster UDGs might be undergoing disruption or may have features that are not modeled by our S-shaped warp, similar to those UDGs observed in the field (Merritt et al. 2016; Román & Trujillo 2017).

⁶ Here we have approximated the Coma cluster as a point mass. Using an NFW halo profile, we find the minimum dark matter fractions to be: 99%, 94%, 82%, and 62% respectively).

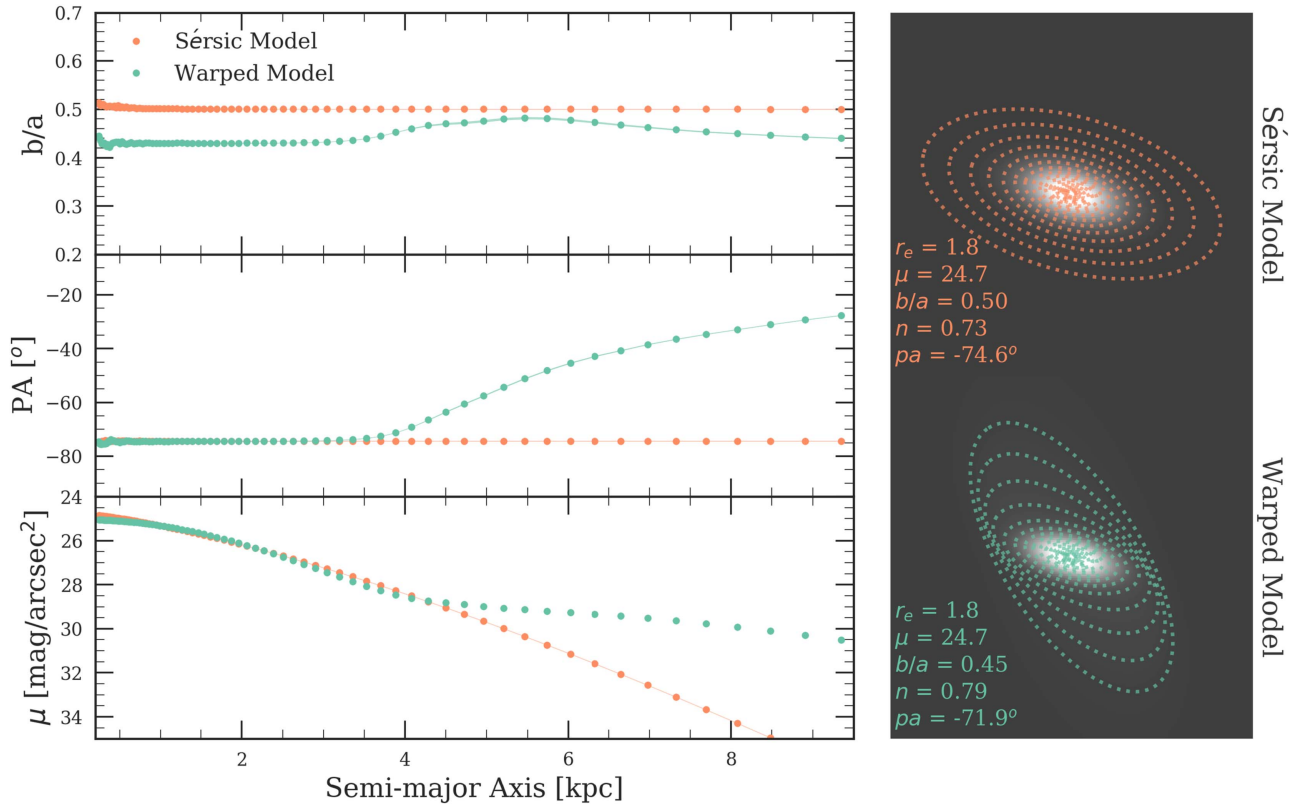


Figure 8. ELLIPSE analysis on individual Sérsic and Warped models. The axis ratio (b/a) and position angle (PA) are constant, and the surface brightness falls smoothly for the Sérsic model. However, a distortion at $r > 2r_e$ is noticed in all three parameters for the Warped model. This feature is observed in brighter warped galaxies as well as in disrupted satellite galaxies in numerical simulations (see Johnston et al. 2002). Due to the low S/N of UDGs, such analysis cannot be done directly on observations.

We note here that our analysis is only sensitive to S-shaped distortions, and we cannot rule out other types of tidal features. Deeper data may provide better constraints for individual galaxies, although sky subtraction issues may limit the analysis unless great care is taken to obtain an optimally flat background in the observations.

We thank the anonymous referee for a very constructive and helpful report. We also thank Johannes Lange for valuable discussion. Support from NSF grant AST-1312376 is gratefully acknowledged.

Appendix Constructing the Warped models

The Warped models are created by adding an inner ellipsoidal model with a fixed position angle to an outer ellipsoidal model whose position angle varies with radius. A Warped model is created for each UDG by adding the inner and outer components with the same center, both of which follow Sérsic light profiles. For each model, we require that the structural parameters, as derived from a single-component fit by GALFIT, are identical to those that are actually measured from the image. This is achieved by creating 100 randomly generated models and choosing the one whose fitted parameters are closest to those derived from the actual UDG image. The parameters we match between the UDG and the model are: effective radius (r_{UDG}), central surface brightness in R -band (μ_{UDG}), Sérsic index (n_{UDG}), and axis ratio (b/a_{UDG}). The direction of the warp of the best-fit model is chosen at random,

with the constraint that there are approximately equal numbers of models with warp in each direction.

The inner component is made by superimposing ellipses at the center. All of the ellipses have the same r_e , μ_0 , b/a , and n , and their values are chosen randomly with the following constraints (parameter subscript “UDG” refers to the parameter value for the UDG being modeled).

1. Inner effective radius: $0.6r_{\text{UDG}} < r_{\text{in}} < r_{\text{UDG}}$.
2. Inner central surface brightness: $\mu_{\text{in}} = \mu_{\text{UDG}}$.
3. Inner Sérsic index: $0.6n_{\text{UDG}} < n_{\text{in}} < n_{\text{UDG}}$.
4. Inner axis ratio: $0.6b/a_{\text{UDG}} < b/a_{\text{in}} < b/a_{\text{UDG}}$.
5. Position angle of the inner ellipses with respect to the major axis of the UDG is zero.

The outer component is made by superimposing ellipses at the center as well, but the various parameters of the ellipses change gradually.

1. Outer effective radius changes linearly from r_{in} to $\sim 3r_{\text{in}}$, with the radius changing by ~ 0.15 kpc/ellipse.
2. Outer central surface brightness: the flux of the center of the ellipse drops off as

$$\mu_{\text{out}} = \mu_{\text{in}} - 2.5 \log_{10}(a \exp(-bN)) \quad (3)$$

where, a and b are random numbers in the range $0.1 < a < 0.9$ and $0.01 < b < 0.05$, respectively, and are allowed to vary between different instances of the model. N refers to the index of the ellipse where $N = 1$ is the innermost ellipse and $N = 100$ is the outermost ellipse.

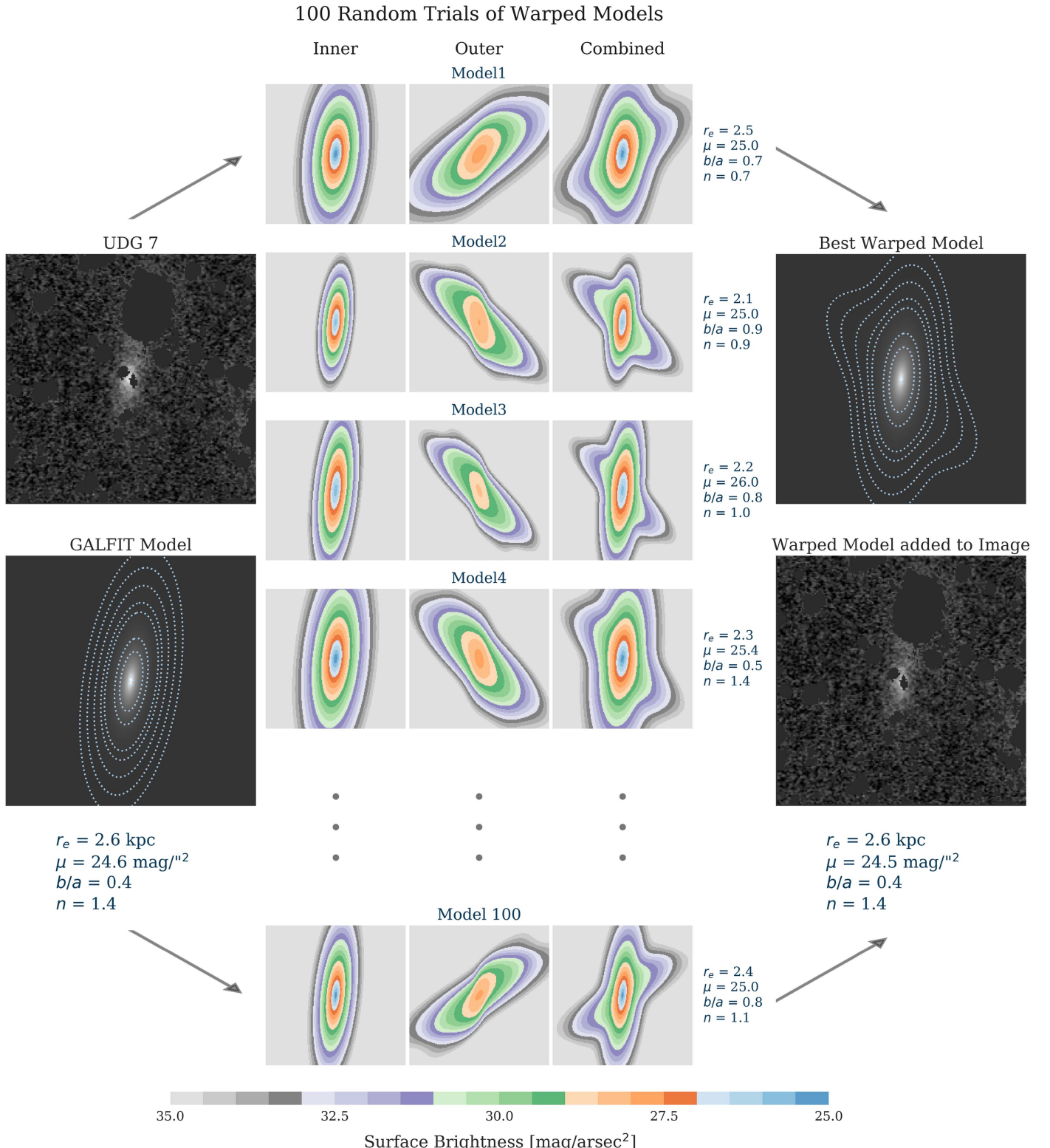


Figure 9. Making of the Warped models. The left panel shows a masked UDG image (top) and the Sérsic model fit by GALFIT (bottom). One hundred Warped models are made for each UDG, each model consisting of an inner component and a warped outer component, as shown in the middle panel. GALFIT is run on all 100 models, and the model with the least difference in values of r_e , μ_0 , b/a , and n between the UDG and the model is chosen. The right panel shows the best-fit Warped model (top) and the Warped model added to the masked image of the sky (bottom).

3. Outer Sérsic index: $0.2n_{\text{in}} < n_{\text{out}} < n_{\text{in}}$
4. Outer axis ratio: $b/a_{\text{out}} = b/a_{\text{in}}$
5. Position angle of the ellipses with respect to the major axis increases linearly from 0° to $\sim 60^\circ$ at a rate of $\sim 3^\circ/\text{ellipse}$.

The inner and outer components are averaged together to produce the combined image with S-shaped outer isophotes (as shown in Figure 7 and Figure 8), akin to the image of Figure 1. After generating the models, they are fit with a single-component

Sérsic profile using GALFIT, and the fit values of r_e , μ_0 , b/a , and n are compared with the values that are measured from the image of the UDG. The model with the smallest difference is chosen as the best Warped model for that UDG (Figure 9). If the best model has one parameter deviating by $>20\%$ from the original value, the whole set of 100 is thrown out and the process is repeated by creating 100 more models until a best-fit model is found where all of the parameters deviate by $<20\%$.

We do not add any noise to these models but do apply their respective masks on them to take into account the effect of masking on the stacked images.

ORCID iDs

- Lamiya Mowla <https://orcid.org/0000-0002-8530-9765>
 Pieter van Dokkum <https://orcid.org/0000-0002-8282-9888>
 Allison Merritt <https://orcid.org/0000-0001-9467-7298>
 Roberto Abraham <https://orcid.org/0000-0002-4542-921X>
 Masafumi Yagi <https://orcid.org/0000-0001-7550-2281>
 Jin Koda <https://orcid.org/0000-0002-8762-7863>

References

- Agertz, O., & Kravtsov, A. V. 2016, *ApJ*, 824, 79
 Amorisco, N. C., & Loeb, A. 2016, *MNRAS*, 459, L51
 Beasley, M. A., Romanowsky, A. J., Pota, V., et al. 2016, *ApJL*, 819, L20
 Beasley, M. A., & Trujillo, I. 2016, *ApJ*, 830, 23
- Bertin, E., & Arnouts, S. 1996, *A&AS*, 117, 393
 Bullock, J. S., & Johnston, K. V. 2005, *ApJ*, 635, 931
 Di Cintio, A., Brook, C. B., Dutton, A. A., et al. 2017, *MNRAS*, 466, L1
 D’Souza, R., Kauffmann, G., Wang, J., & Vegetti, S. 2014, *MNRAS*, 443, 1433
 Johnston, K. V., Bullock, J. S., Sharma, S., et al. 2008, *ApJ*, 689, 936
 Johnston, K. V., Choi, P. I., & Guhathakurta, P. 2002, *AJ*, 124, 127
 King, I. 1962, *AJ*, 67, 471
 Koch, A., Burkert, A., Rich, R. M., et al. 2012, *ApJL*, 755, L13
 Koda, J., Yagi, M., Yamanoi, H., & Komiyama, Y. 2015, arXiv:1506.01712
 Kubo, J. M., Stebbins, A., Annis, J., et al. 2007, *ApJ*, 671, 1466
 Merritt, A., van Dokkum, P., Danieli, S., et al. 2016, *ApJ*, 833, 168
 Okabe, N., Futamase, T., Kajisawa, M., & Kuroshima, R. 2014, *ApJ*, 784, 90
 Peng, C. Y., Ho, L. C., Impey, C. D., & Rix, H.-W. 2002, *AJ*, 124, 266
 Peng, C. Y., Ho, L. C., Impey, C. D., & Rix, H.-W. 2010, *ApJ*, 139, 2097
 Peng, E. W., & Lim, S. 2016, *ApJL*, 822, L31
 Penny, S. J., Conselice, C. J., de Rijcke, S., & Held, E. V. 2009, *MNRAS*, 393, 1054
 Román, J., & Trujillo, I. 2017, *MNRAS*, 468, 703
 Searle, L., & Zinn, R. 1978, *ApJ*, 225, 357
 Tal, T., & van Dokkum, P. G. 2011, *ApJ*, 731, 89
 van der Burg, R. F. J., Muzzin, A., & Hoekstra, H. 2016, *A&A*, 590, A20
 van Dokkum, P., Abraham, R., Brodie, J., et al. 2016, *ApJL*, 828, L6
 van Dokkum, P., Whitaker, K., Brammer, G., et al. 2010, *ApJ*, 709, 1018
 van Dokkum, P. G., Abraham, R., Merritt, A., et al. 2015a, *ApJ*, 804, 1
 van Dokkum, P. G., Romanowsky, A. J., Abraham, R., et al. 2015b, *ApJ*, 804, 1
 Yagi, M., Koda, J., Komiyama, Y., & Yamanoi, H. 2016, *ApJS*, 225, 11
 Yozin, C., & Bekki, K. 2015, *MNRAS*, 452, 937
 Zibetti, S., White, S. D. M., & Brinkmann, J. 2004, *MNRAS*, 347, 556